Nuclear Instruments and Methods in Physics Research A 1075 (2025) 170403

Contents lists available at ScienceDirect

Nuclear Inst. and Methods in Physics Research, A

journal homepage: www.elsevier.com/locate/nima

Full Length Article

Preparation of lanthanide thin films for ion beam experiments and post irradiation characterization

E. Artes [a,b,c,*], D. Ackermann [d], Ch.E. Düllmann [a,b,c], T. Häger [e], B. Kindler [c], T. Lefrou [d], B. Lommel [c], A.T. Loria Basto [a,b], C.-C. Meyer [a,b], C. Mokry [a,b], F. Munnik [f], J. Piot [d], L.E. Reed [a], D. Renisch [a,b], H. Rothard [g], J. Runke [a,c], H. Savajols [d], C. Stodel [d], T. Madi [g], V. Urbanova [a], V. Watt-Morel [d], A. Yakushev [c]

[a] Department Chemie - Standort TRIGA, Johannes Gutenberg-Universität Mainz, Fritz-Strassmann-Weg 2, 55128 Mainz, Germany
[b] Helmholtz-Institut Mainz, Staudingerweg 18, 55128 Mainz, Germany
[c] GSI Helmholtzzentrum für Schwerionenforschung GmbH, Planckstraße 1, 64291 Darmstadt, Germany
[d] GANIL, CEA/DRF-CNRS/IN2P3, Bd. Henri Becquerel, BP 55027, F-14076 Caen, France
[e] Institut für Geowissenschaften, Johannes Gutenberg-Universität Mainz, Johann-Joachim-Becher-Weg 2, 55128 Mainz, Germany
[f] Helmholtz-Zentrum Dresden-Rossendorf, Bautzner Landstraße 400, 01328 Dresden, Germany
[g] CIMAP, CEA-CNRS-ENSICAEN-UNICAEN Bd. Henri Becquerel, Caen, France

ARTICLE INFO

Keywords:
Triflate
Electrochemical deposition
Thin film deposition
Irradiation
Ion beam
Vibrational spectroscopy
Ion beam analysis

ABSTRACT

The heaviest elements in the periodic table have a low production yield. In order to increase the production yield of the superheavy elements, thicker targets are required than the present molecular plating technique can offer. Therefore, lanthanide thin films, as lighter homologues to the actinides, were prepared by a new electrodeposition method. The trifluoromethanesulfonates (triflates) of the lanthanide salts were dissolved in Dimethylformamide (DMF) and then electrochemically deposited onto substrates of different geometries. These thin films were irradiated with different swift heavy ion beams with energies of over 200 MeV. Thin films were analyzed spectroscopically by Raman and IR measurements before and after irradiation, to investigate chemical changes induced by irradiation.

1. Introduction

The heaviest elements in the periodic table, superheavy elements (SHE), are produced by nuclear fusion reactions induced by intense heavy-ion beams with energies around the Coulomb barrier [1,2]. In this process, a target, often a thin film of an actinide, is irradiated with ^{48}Ca [1]. The SHE production rate depends on the cross section of the nuclear reaction of the ion beam projectile and the target atom of the target layer. Additionally, the production rate also depends on the beam intensity and the target thickness and is small for the SHE. To increase the production rate, the intensity of the ion beam or the layer thickness of the target has to be increased. The cross section function limits the maximum layer thickness to roughly 1500 $\frac{\mu g}{cm^2}$ [3]. Layer thicknesses above 1500 $\frac{\mu g}{cm^2}$ would barely increase the production yield of SHE.

Nowadays, the standard method for the production of actinide films is molecular plating, which is an electrochemical deposition method [4–6]. However, the film thickness that can be reliably achieved with this method is limited to about 1000 $\frac{\mu g}{cm^2}$ on the thin substrates [4,7].

Recently, however, a method using salts of the trifluoromethanesulfonic acid (triflic acid), which is a super acid, and dimethylformamide (DMF) in electrochemical deposition was reported. By dissolving the lanthanide oxides in triflic acid and dissolving the newly formed trifluoromethanesulfonate (trilfate) salt in an aprotic organic solvent like DMF, layer thicknesses of up to 2000 $\frac{\mu g}{cm^2}$ for lanthanides could be achieved. The first experiments with these lanthanide targets have already been proven to be stable in a ^{48}Ca ion beam with 6 $\frac{MeV}{u}$ and an accumulated fluence of 3.9×10^{14} $\frac{ions}{cm^2}$ [8].

The aim of this work is to understand how these thin films change chemically in the ion beam, by characterization via infrared (IR) and Raman spectroscopy both before and after irradiation. Additionally, Rutherford backscattering (RBS) combined with proton-induced X-ray emission spectroscopy (PIXE) was used to analyze the elemental composition of the thin layers.

* Corresponding author at: Department Chemie - Standort TRIGA, Johannes Gutenberg-Universität Mainz, Fritz-Strassmann-Weg 2, 55128 Mainz, Germany.
E-mail address: erartes@uni-mainz.de (E. Artes).

https://doi.org/10.1016/j.nima.2025.170403
Received 12 December 2024; Received in revised form 3 March 2025; Accepted 3 March 2025
Available online 18 March 2025

2. Experimental methods

2.1. Target production

Commercially available trifluoromethanesulfonate (triflate) and self-produced triflates of terbium and thulium were used for the production of thin films.

The salts were dissolved in organic solvents and then deposited potentiostatically on titanium foils with different thicknesses.

Multiple targets were produced for different experiments, including ion beam irradiation conducted at the Grand Accélérateur National d'Ions Lourds (GANIL), France, and Transactinide Separator and Chemistry Apparatus (TASCA) at GSI Helmholtzzentrum für Schwerionenforschung, Germany, as well as for the Helmholtzzentrum Dresden Rossendorf (HZDR), Germany, where the Rutherford Backscattering and Proton Induced X-ray Emission (RBS/PIXE) measurements of the thin films were carried out.

2.1.1. Preparation of lanthanide stock solution

Lanthanide triflates were prepared as described in [8,9]. 15-50 mg lanthanide oxide were heated with a small stochiometric excess of triflic acid and water was then evaporated to dryness. This way, the lanthanide triflate salts $[Ln(H_2O)_9][CF_3SO_3]_3$ (Ln = Tb, Tm) were obtained.

$$Ln_2O_3 + 6\,CF_3SO_3H + 15\,H_2O \longrightarrow 2\,[Ln(H_2O)_9](CF_3SO_3)_3 \ (Ln = Tb,\ Tm)$$

In parallel, commercial anhydrous triflate salts $Ln(TfO)_3$ (Ln = Tb, Tm), [Merck GmbH] were used.

The salts were dissolved in DMF to obtain a stock solution with varying concentrations between 500–1000 $\frac{\mu g}{mL}$.

2.1.2. Preparation of terbium targets for GANIL

An aliquot of the stock solution with the desired amount of terbium was diluted in DMF. The goal was to produce targets with a layer thickness of 1500–2000 $\frac{\mu g}{cm^2}$. For the production of the thin films two different electrochemical cells were used.

The cylindrical chimney cell (Fig. 1a) is constructed from a titanium block, with the substrate connected as the cathode. The cell wall, made of polyether ether ketone (PEEK), features a circular opening with a diameter of 10 mm, resulting in a deposition area of 0.785 cm^2. An ethylene propylene diene monomer (EPDM) gasket was used. The volume of the cell holds 10 mL. A palladium anode was used in these experiments. With the aim of quantitatively depositing 2000 $\frac{\mu g}{cm^2}$, 1570 µg of terbium were used.

The prepared solution was then deposited galvanostatically at a constant current and current density of ≈2.5 $\frac{mA}{cm^2}$ for 2 h. Titanium foils with thicknesses of 2.1–2.3 µm and 10 µm were used as substrates for the deposition.

2.1.3. Preparation of thulium targets for TASCA

Since the triflate method uses DMF and DMSO as solvents, which are less viscous than the isobutanol/isopropanol mixture used in the molecular plating technique, the existing cell [10] used to produce the TASCA targets [11] was not leak-tight. The cell was slightly modified for this reason. The newly modified cell (Fig. 1b and c) consists of one block of PEEK, one wall with a 6 cm^2 banana-shaped opening that extends outwards along the edge to hold a gasket of the same shape, made of EPDM. At this position, the target substrate, which was glued to the TASCA frame with a silver epoxy glue, was mounted to the wall and fixed with a stainless steel back plate with five screws. This back plate also acted as an cathode. The anode was placed across the target in the cell with a crocodile clip. As the surface area of the cathode is relatively large, a rectangular graphite anode measuring 40 × 30 mm was used in these experiments. This consists of fewer parts than the standard version [7], therefore it is resistant to leakage.

The "TASCA cell" has a volume of 35 mL and the deposition area is banana-shaped with a deposition area of 6 cm^2 so that four segments form one target wheel with a diameter of 10 cm. This wheel was rotated in TASCA, to distribute the energy deposition of ion beam on a higher surface to prevent the destruction of targets [7].

With the aim of quantitatively depositing 2000 $\frac{\mu g}{cm^2}$ thickness layer, 1200 µg of thulium were used. Due to the different volumes and concentrations, which were chosen due to the deposition area and size of the anode compared to the chimney cell, the parameters had to be adjusted for the best deposition result. The adjusted solution was then galvanostatically deposited at a current density of approximately 3 $\frac{mA}{cm^2}$, for 5 h. From this solution, several depositions were made, each on a 2.1 µm thick titanium foil.

2.1.4. Preparation of thulium targets for measurements at HZDR

Commercial thulium triflate was deposited on 25 µm thick titanium foil. The chimney setup was used with an opening diameter of 6 mm, which results in a deposition area of 0.28 cm^2. A glassy carbon anode with 1 mm diameter and 5 cm length was used. With the aim of quantitatively depositing 2000 $\frac{\mu g}{cm^2}$, 560 µg of thulium were used.

Unlike the targets for GANIL and TASCA, the samples were prepared in argon atmosphere using dry solvents. The O_2 concentration in the box varied between 1 and 3 ppm, the H_2O concentration in the atmosphere was below 1 ppm. CO_2 concentration could not be measured.

The samples were then analyzed at the HZDR using Elastic Recoil Detection Analysis (ERDA), PIXE and RBS.

2.1.5. Tracer production of terbium and thulium

The electrochemical deposition yields were determined by the production of terbium and thulium tracers with neutron capture reactions. For this purpose terbium oxide and thulium oxide were irradiated in the TRIGA Mainz research reactor at a neutron flux of $7 \times 10^{11}\ \frac{n}{cm^2\,s}$ for 1 h, producing ^{160}Tb and ^{170}Tm. These oxides were transformed to the triflate salts and deposition experiments were done, as described in 2.1.1 and 2.3.1, respectively.

2.2. Target irradiation

The manufactured targets were irradiated at GSI using the TASCA setup with ion beam provided by the UNIversal Linear ACcelerator (UNILAC) and at GANIL's D1-SME beamline using cyclotron beams. Different ion beams and energies were used in the respective facilities (Table 1).

2.2.1. Irradiation experiments at GSI TASCA

Self made thulium triflate thin films for TASCA irradiation were prepared on 2.1 µm titanium foils provided by the GSI target laboratory. One thin film was prepared with DMSO, while the others were prepared with DMF. Four targets were mounted on a wheel (Fig. 2) with a total target area of 24 cm^2.

This wheel was mounted in TASCA and the targets were irradiated with ^{48}Ca with an energy of 4.8 $\frac{MeV}{u}$ and a particle flux of 2.7×10^{12} pps for 40 min. The beam is collimated to 9 mm diameter just in front of the targets. The typical flux distribution is Gaussian with a FWHM of 8 mm. The ion beam passed through the titanium foil before hitting the thulium thin films, to keep the same layer sequence as in the production of superheavy elements. During irradiation, the targets were constantly rotated at 37.5 Hz [11] for even distribution of the ion beam on all the targets. This resulted in a fluence of $2.7 \times 10^{14}\ \frac{ions}{cm^2}$ for all targets.

2.2.2. Irradiation experiments at GANIL

Self-made terbium triflate was used to produce thin films on 2.1 µm thick titanium foils, which were provided by the GSI target laboratory. The thin films were produced in circular shape as previously described and glued afterwards on frames, provided by GANIL (Fig. 3). The wheel

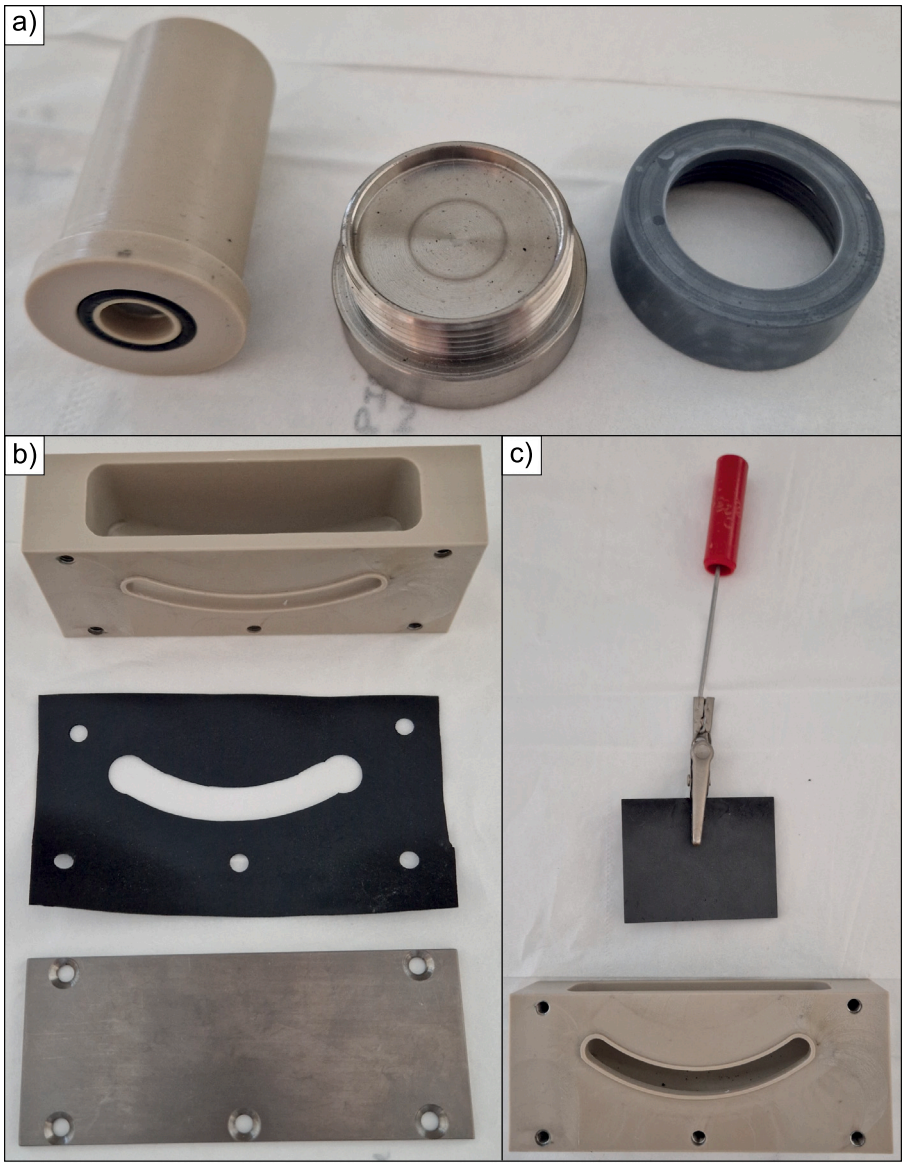

Fig. 1. The cells used for the preparation of targets. (a) The chimney cell used to prepare targets for GANIL and HZDR. It is also made out of PEEK. Next to it are the titanium base and a fixing nut made out of polypropylene. (b) The dismantled cell for TASCA targets. The cell used to prepare targets for TASCA is made out of PEEK. The sealing mat is made out of EPDM and the back is made out of stainless steel. (c) The TASCA cell with the used graphite anode.

Table 1
Overview of the different target irradiations. Three similar targets were irradiated at GANIL with an ^{70}Zn ion beam with an projectile energy of 9.3 $\frac{\text{MeV}}{\text{u}}$. Each target received a different fluence. Four similar targets were irradiated at TASCA at GSI with an ^{48}Ca ion beam. The beam had an energy of 4.9 $\frac{\text{MeV}}{\text{u}}$ and all targets received the same fluence. At HZDR three targets were irradiated with a ^{35}Cl beam. The energy was 1.2 $\frac{\text{MeV}}{\text{u}}$. The aim was ERDA measurements with the Cl beam so no effort was made to keep the fluence identical.

Facility	Element	Target names	Target form	Beam	Projectile energy [$\frac{\text{MeV}}{\text{u}}$]	Fluence [10^{13} $\frac{\text{ions}}{\text{cm}^2}$]
GANIL	Terbium	GANIL-Tb-1 GANIL-Tb-2 GANIL-Tb-3	Circular 10 mm	^{70}Zn	9.3	1.0(1) 9.5(9) 100(10)
GSI	Thulium	GSI-Tm-1 GSI-Tm-2 GSI-Tm-3 GSI-Tm-4	Banana shaped	^{48}Ca	4.9	27(2)
HZDR	Thulium	HZDR-1 HZDR-2	Circular 6 mm	^{35}Cl	1.2	4.7(5) 3.7(4)
–	Terbium	Control 1	Circular 6 mm	–	–	–

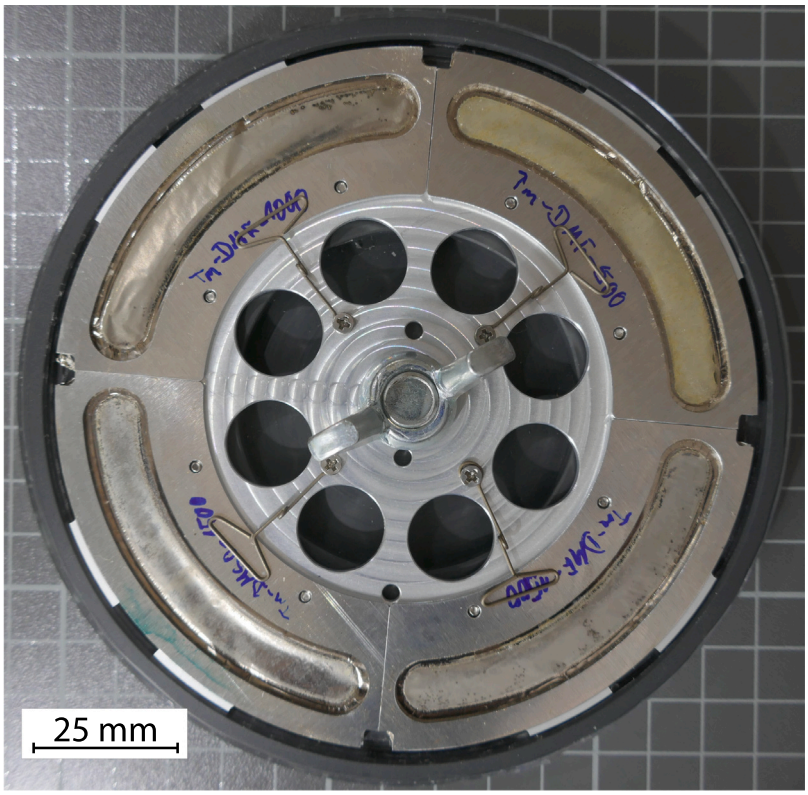

Fig. 2. The TASCA setup is made out of four targets arranged on a wheel with a diameter of 10 cm [11]. Each segment has an area of 6 cm^2. The wheel shown was mounted in TASCA and irradiated with an ^{48}Ca ion beam.

consists of three aluminum segments. Each segment supports up to four targets [12]. At GANIL the targets were irradiated with a ^{70}Zn ion beam an energy of 9.3 $\frac{MeV}{u}$ and a varying particle flux of 0.5–1.5 $\times 10^{10}$ pps. The ion beam passed through the titanium foil before hitting the terbium thin films. The wheel was not rotated during the irradiation and each target was exposed to the beam for a defined period. A magnetic sweeping device is used to assure uniform irradiation on a rectangular irradiation field (defined by 4 movable slits) of up to 5 cm × 5 cm. The diameter of the ion beam was 6×7.5 mm^2 before sweeping. The ratio of the sweeping frequencies (horizontal frequency: ≈400 Hz; vertical frequency: ≈40 Hz) is chosen so, that no regular spatial structures such as Lissajous figures can occur. The projectile ion flux on the target is monitored during the irradiation by a secondary electron emission detector (stack of thin foils) allowing to measure the secondary electron current induced by the projectile. Prior to the target irradiation, a Faraday cup is inserted and the ratio of the secondary electron current and the projectile current is measured. This procedure allows a precise measurement of the projectile ion flux and the accumulated projectile fluence with an accuracy of ≈5% [13]. The fluences deposited on the individual targets varied between 1×10^{13} and 1×10^{15} $\frac{ions}{cm^2}$. The fluence of the individual target is also noted in Table 1.

2.3. Target analysis

To determine the efficiency of the deposition, tests with radioactive terbium were carried out beforehand. This will be described in Section 2.3.1.

The films were also examined under a scanning electron microscope to determine the morphological changes.

To chemically characterize the films, IR and Raman spectra of the irradiated TASCA and GANIL films, as well as the non-irradiated ones; were obtained at the Institute of Geosciences institute of the Johannes Gutenberg University in Mainz.

2.3.1. Yields

The yield is the amount of lanthanide deposited on the surface, compared to the amount in the solution. A yield of 100% is achieved, if no lanthanide remains in the solution after deposition.

To determine the deposition yield, ^{160}Tb and ^{170}Tm tracers were produced by neutron activation at the TRIGA Mainz research reactor as described in Section 2.1.5.

An Aliquot of the supernatant solution was taken in order to make an indirect yield measurement via gamma spectroscopy. This was done before and after deposition. The gamma activity of the samples was measured in an HPGe detector from Ortec and the gamma spectra were evaluated with the Genie 2000 software from Canberra. The difference in the activities of the supernatant solution before and after deposition was determined by giving indirect information on the deposition yield, neglecting potential losses to sorption on the container walls. The experiment was replicated five times to assess reproducibility and facilitate error estimation. For the ion beam experiments, inactive targets were produced in the same way. Yields were assumed to be in the same order as in the tests with the radioactive isotopes.

2.3.2. Scanning electron microscopy (SEM)

To evaluate the quality of the films, the samples were examined by scanning electron microscopy (Philips XL30) using an accelerating voltage of 20 kV and detectors for secondary (SE) and back scattered electrons (BSE).

Pictures of the thin films were acquired after the irradiation. Fresh thin films were produced and compared to the irradiated ones, to see the impact of the ion beams on the morphology.

2.3.3. Infrared microscopy (IR)

The targets GANIL-Tb-2, DMF-1 and Control-1 were analyzed by infrared microscopy (Nicolet Continuμm connected to a Nicolet 6700, THERMO SCIENTIFIC). A mercury cadmium telluride (short: MCT) detector was used. The increments were set to 0.1 nm and the acquisition

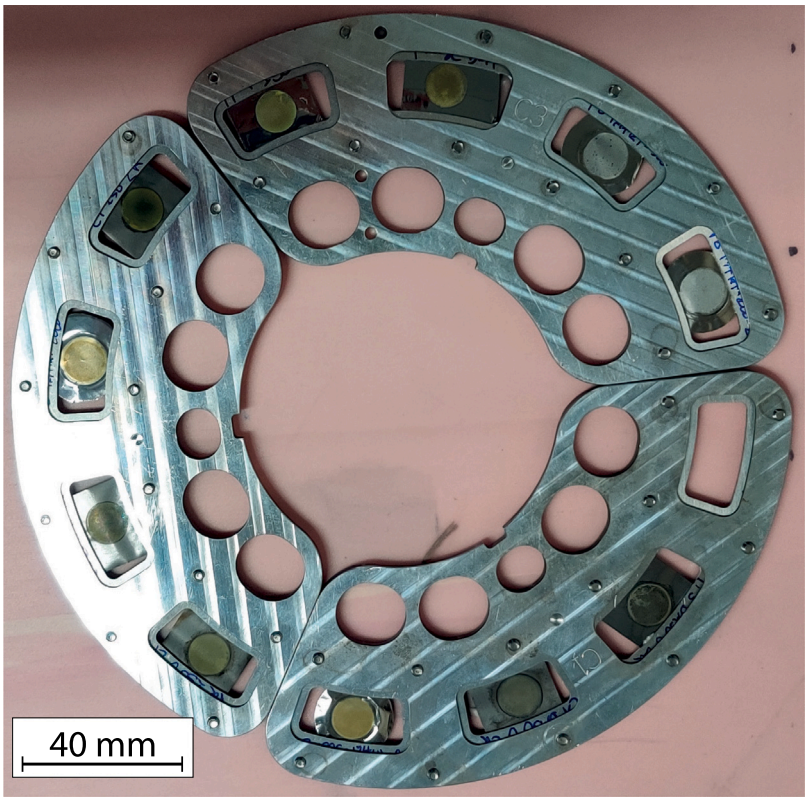

Fig. 3. Target wheel used for irradiation tests at GANIL. The wheel consists of three segments. Each segment supports up to four target. One position was left intentionally blank for the beam analysis.

time for each spectrum was set to 5 min. Infrared spectra from 500 cm^{-1} to 4000 cm^{-1} were collected in reflection on a gold mirror. IR spectra were recorded from three different locations from each thin film to exclude artifacts in the film. The reflection of IR radiation from the sample was measured.

2.3.4. Confocal Raman microscopy

The same targets, from Section 2.3.3 were also analyzed with a confocal Raman microscope (Horiba Jobin Yvon LabRAM HR 800 spectrometer). The microscope was equipped with a Si-based charge-coupled device (CCD) detector (Peltier-cooled), an integrated Olympus BX41 optical microscope and an automatized x-y stage. A 50x long-distance objective (numerical aperture 0.55), a frequency-doubled Nd:YAG laser with 532.21 nm emission wavelength, a grating with 1800 $\frac{\text{grooves}}{\text{mm}}$, and a slit width of 100 μm were used to acquire the data. The spectral resolution was 0.6 cm^{-1}. Raman spectra of the different thin films from 200 cm^{-1} to 3200 cm^{-1} were collected.

2.3.5. Elastic Recoil Detection Analysis (ERDA)

The samples HZDR-1, HZDR-2 and HZDR-3 were analyzed with Elastic Recoil Detection Analysis (ERDA) using a 43 MeV $^{35}Cl^{7+}$ ion beam. The angle between the sample normal and the incoming beam was 75°, the scattering angle was 30°. The analyzed area was about 2 × 2 mm^2. The recoil atoms and scattered ions were detected with a Bragg Ionization Chamber (short BIC), which enables energy measurements and Z identification of the particles. H recoils were detected with a separate solid-state detector at a scattering angle of 40°. In front of this detector a 25 μm Kapton foil was mounted to stop scattered ions and heavy recoil ions. The depth resolution of this system is limited by the energy loss straggling in the foil. The ion-beam dose (in arbitrary units) was determined using a gold plated rotating (1 Hz) vane and a solid-state detector, which detected Cl backscattering from Au. Irradiation at the ERDA setup of the HZDR inflicted an ion dose per area of up to $I = 1.6(2) \times 10^{14}$ $\frac{\text{ions}}{\text{cm}^2}$ to the thin films. The aim was ERDA measurements with the Cl beam so no effort was made to keep the fluence for all targets identical. This induced changes in the sample surface visible to the naked eye. The changes in the thin films of the ERDA measurements could be characterized using μBeam, so irradiated and non-irradiated surfaces could be compared.

2.3.6. μBeam

The same samples analyzed by ERDA were also examined using Rutherford Backscattering Spectrometry (RBS) in combination with Particle Induced X-ray Emission (PIXE), employing a 3 MeV H^+ beam. The ion beam was focused to a spot size of (7 × 5) μm^2. Backscattered protons were detected at a scattering angle of 174° using a silicon strip detector, while a Ketek silicon drift detector with an 80 μm^2 collimation was used to detect X-rays emitted from the sample. This detector was positioned outside the sample chamber, separated by a 1 μm silicon-nitride window, a 6 mm air layer, and a 25 μm Be window. Additionally, a 65 μm aluminum absorber was employed to minimize Ti-K X-ray contributions and block backscattered H^+ ions from entering the detector. RBS provided depth profiles for major elements, excluding hydrogen, which RBS cannot detect. For C, N, and O, evaluated cross-sections from SigmaCalc were applied [14]. For titanium, accurate data for the energy range and scattering angle of this study were unavailable, so a measurement on the Ti backing foil was used to obtain non-Rutherford cross-sections through the program ndf [15].

AFM measurements on the blank titanium foil revealed significant roughness with value of rms = 39(8) nm. Consequently, the determined cross-section may not be universally applicable. The titanium foils used for the investigations at the HZDR correspond to the technical standard in target production, which includes their known surface roughness.

For the thulium thin films, initial large scans, with a size of (260 × 260) μm^2 or (260 × 205) μm^2, were performed, followed by point measurements with the size of the beam spot mentioned

Table 2
The desired deposition mass, yields and layer thicknesses of the described targets.

Target names	Desired layer thickness [μg/cm^{-1}]	Yield	Real layer thickness [μg/cm^{-1}]
GANIL-Tb-1	2000	78(5)%	1560(100)
GANIL-Tb-2		81(5)%	1620(100)
GANIL-Tb-3		82(5)%	1640(100)
GSI-Tm-1	2000	23(2)%	460(40)
GSI-Tm-2		26(2)%	520(40)
GSI-Tm-3		23(2)%	460(40)
GSI-Tm-4		25(2)%	500(40)
HZDR-1	2000	–	–
HZDR-2			
Control-1	2000	–	–

above in a homogeneously composed region. The μBeam analytics were performed on the irradiated samples with the ERDA procedure. The analysis area between the irradiated and non-irradiated regions of the sample surface was examined, allowing both areas to be analyzed within a single image to study the effects of ion radiation on the thin films.

3. Results

3.1. Yields

The yields were determined using tracer activation of terbium and subsequent gamma measurement of the supernatant solutions before and after deposition.

The aim was to produce thin films with an areal weight of 1500–2000 $\frac{\mu g}{cm^2}$.

The thin films of the TASCA targets were produced with inactive thulium. Fig. 2 does not allow to infer details of the layer uniformity. There are a few smaller areas visible, where the layer is thinner (or even absent) compared to the average, but overall, uniformity is similar to that obtained in the classical MP method. After the deposition, the supernatant solution was activated, and after quantification, it was found that, that the residual concentration of thulium in this solution corresponds to a thin layer of a thickness of approximately 500 $\frac{\mu g}{cm^2}$. Further experiments with the TASCA cell showed that thin films with 1600 ± 100 $\frac{\mu g}{cm^2}$ could also be produced with adjustments to higher current densities of 3 $\frac{mA}{cm^2}$ for 3 h in the deposition process, which corresponds to a yield of $(80 \pm 5)\%$.

For the circular targets, the parameters were optimized by adjusting the current density to 2.5 $\frac{mA}{cm^2}$ for 2 h and a constant yield of $(80 \pm 5)\%$ was also achieved. These settings were used to produce inactive targets for GANIL. The yields for all targets are listed in Table 2. The yields were not determined for HZDR-1, HZDR-2 and Control-1.

3.2. Irradiation results

All targets were able to mechanically withstand the conditions in the ion beams. The targets irradiated at TASCA were radioactive afterwards, their final analytics were performed in non-radiation licensed laboratories after a waiting time of one year, at which time the activity had decayed sufficiently.

While the targets that were irradiated at TASCA had completely decayed at the time of the analytical measurements, some targets that were irradiated in GANIL were still active. The highest fluence that one target experienced at GANIL was 1×10^{15} $\frac{ions}{cm^2}$. This target still had residual activity after irradiation, which is why no Raman and IR data could be collected from this target. Instead, targets with a fluence of 1×10^{14} $\frac{ions}{cm^2}$ were characterized. Table 3 is an overview, which shows the analytical methods used for the targets described in this work.

Table 3
Overview of the applied analytics on the specific target.

Target names	Lanthanide	Analytical method
GANIL-Tb-2	terbium	IR, Raman
GSI-Tm-1	thulium	IR, Raman
HZDR-1	thulium	μbeam
Control 1	terbium	IR, Raman

Table 4
Ion beam doses of different irradiations in Gray. ^{35}Cl was used at ERDA measurements at HZDR, ^{48}Ca was used at TASCA and ^{70}Zn at GANIL for irradiation tests. dE/dx elec. stand for the energy loss due to electric interactions.

Isotope	^{35}Cl	^{48}Ca	^{70}Zn
Energy per nucleon [MeV/u]	1.2	4.90	9.28
dE/dx elec. [keV/nm]	7.8	8.9	12
Fluence [10^{14} ions/cm^2]	2.0(2)	2.7(3)	1.0(1)
Energy dose [Gy]	$2.9(3) \times 10^8$	$4.5(5) \times 10^8$	$2.5(3) \times 10^8$

3.2.1. Normalization of irradiation effects of the different used beams

Different projectiles and energies were used to irradiate the targets. To be able to compare the irradiated targets to each other it is necessary to normalize the irradiation effect of the different ions beams. This can be done by calculating the energy dose deposition from the ion beams on the targets. The calculations were based on the stopping power of the ions through the thin films simulated by SRIM (version SRIM-2008.04). Necessary for the calculation is an assumption of the density and chemical composition of the target material, the energy of the projectile and fluence of the ion beam. It was assumed, that the target material had the density and chemical composition of the oxides Tm_2O_3 and Tb_4O_7, since the ion beam has the highest energy deposition in the oxides and the actual composition and density are not well known. Furthermore, the energy loss of the ion beam due to the penetration of the titanium foil was taken into account in the calculation for the GSI-Tm-4 and GANIL-Tb-2 targets prior to the calculation of the dose for the target layer. For HZDR-1, however, this was not considered, as the ^{35}Cl beam directly struck the target layer without first penetrating the titanium layer.

The fluence and energy of the ion beam were known. The nuclear and electrical interaction of the projectile with the target material as well as the density were necessary for the calculation of the energy dose deposition. While the electrical interaction leads to an energy loss of the projectile in the target material of $\approx 8 - 12$ $\frac{keV}{nm}$, the nuclear interactions are in the order of 1.0×10^{-2} $\frac{keV}{nm}$ and have less than 1 % impact on the overall dose. The results are visible in Table 4.

3.2.2. Morphology

After irradiation, the targets were examined both with the naked eye and in the SEM. Photographs of the targets before and after their irradiation are shown in Fig. 4. The targets, which received a dose of 10^8 Gy show visible changes in their morphology. GSI-Tm-1 became darker, while HZDR-1 clearly shows a square spot, where the ion beam hit the thin film. GANIL-Tb-2 shows no significant change in the thin film.

SEM images are shown in Fig. 5. The image of the non-irradiated samples show the typical cracks from the electrodeposition procedure. These are similar to the "mudcracking" effect of the molecular plated thin films.

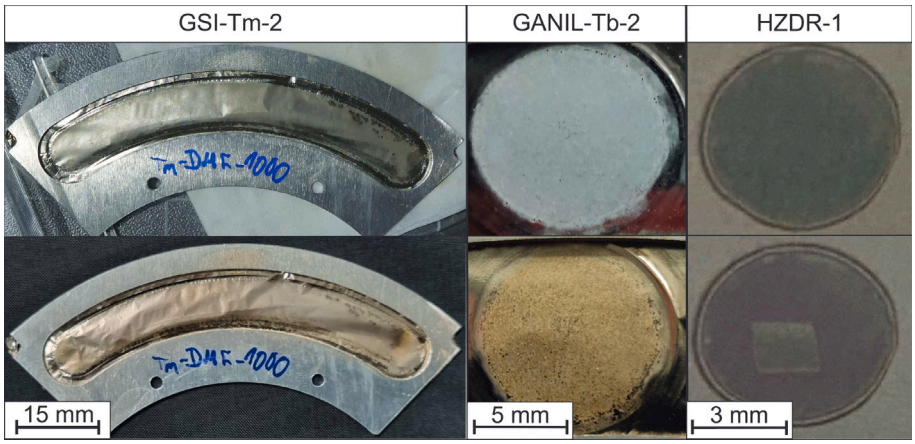

Fig. 4. The top row shows the targets before they were irradiated. The bottom row shows the same targets after irradiation. The detail to the irradiation can be found in Table 1. On the left GSI-Tm-2 before and after irradiation with 2.68×10^{14} ^{48}Ca $\frac{\text{ions}}{\text{cm}^2}$ at TASCA. This target is shown, since a part of GSI-Tm-1 was cut out on purpose for IR and Raman spectroscopy. In the middle GANIL-Tb-2, which was irradiated with 1×10^{14} ^{70}Zn $\frac{\text{ions}}{\text{cm}^2}$ at GANIL. On the right HZDR-1 which was irradiated with 2×10^{14} ^{35}Cl $\frac{\text{ions}}{\text{cm}^2}$s.

The targets that were irradiated at TASCA show optical changes. There was a discoloration of the thin films to black. This is not observed with targets that were irradiated in GANIL. Optical changes were also observed after the irradiation with ^{35}Cl at the HZDR. The square irradiation spot is clearly visible on the target.

The thin films of the irradiated samples show the same structures in the SEM as the non-irradiated targets. Observable is the lack of notable alterations in the morphological composition of GANIL targets, manifesting at both macroscopic and microscopic scales. While TASCA targets exhibit discernible optical alterations, the corresponding changes in SEM imagery are relatively minor. Conversely, notable microstructural variations are evident in targets exposed to ^{35}Cl irradiation at HZDR, notably substantial tile shrinkage in SEM images within the irradiated zones.

3.3. Vibrational spectroscopy

The vibrational spectra of the different targets were measured at the Institute of Geoscience at JGU Mainz.

The Raman spectra of the non-irradiated and irradiated thin films are shown in Fig. 6. Oxides are visible at a Raman shift below 500 cm^{-1} [16]. These also remain visible after irradiation with a dose of $4.5(5) \times 10^8$ Gy of ^{48}Ca or $2.5(3) \times 10^8$ Gy of ^{70}Zn. Carbonate bands can be seen between 680 and 850 cm^{-1}, between 1050 and 1580 cm^{-1}, between 1310 and 1380 cm^{-1}, and between 1580 and 1610 cm^{-1}. These are still visible after irradiation [17,18], but decreased significantly. The bands at 2850 and 2960 cm^{-1} are consistent with the literature on formates and are therefore assigned to this functional group. Their intensity also decreases after irradiation and they become broader, so that only one band is visible after irradiation. The position and assignment of the bands are given in Table 5.

Fig. 7 displays the IR spectra of Control-1, GSI-Tm-1 and GANIL-Tb-2. In both cases, before and after irradiation terbium thin films exhibit a broad band around 3400 to 3550 cm^{-1}. This band is assigned to hydroxide. After the ^{48}Ca irradiation, this band disappears.

The bands within the 1300 to 1700 cm^{-1} range are identified as carbonates [18–20], including vibrations of formates observed in previous studies [21–24] on molecular plated thin films. Another carbonate band appears at 850 cm^{-1} [18–20]. With increasing irradiation intensity, these bands also decrease in intensity. At 2350 cm^{-1} a small band is visible which is a measurement artifact from the titanium background.

Table 5
Assignment of the chemical compounds to the vibrational bands in the IR (Fig. 7) and Raman spectra (Fig. 6) and there corresponding references.

Chemical species	Symbol	IR band [cm^{-1}]	Raman band [cm^{-1}]	Assignment references
Oxide	O	–	315 405–430	[16]
Carbonate	C	850 1300–1700	680–850 1050–1580 1310–1380 1580–1610	[17–20]
Formate	F	1300–1700	2850 2960	[21–24]
Residue water hydroxide	H	3400–3550	–	[25]

3.4. ERDA and μBeam

The fluence induced by ERDA almost corresponds to the fluence at the TASCA setup. Thin films made from commercial triflate under glovebox conditions of Section 2.1.4 changed their morphology (Fig. 8) under ERDA irradiation. Since for ERDA a clearly focused square beam spot has been used, which is visible even to the naked eye (Fig. 8a), the difference between analyzed (i.e., irradiated) and non-analyzed thin film was investigated using the μBeam setup. The PIXE image (Fig. 8b) shows the distribution of thulium in the thin film, the upper third shows the irradiated part, the lower two thirds the non-irradiated film. The image shows irradiation changes in the morphology. After irradiation, the thulium contained in the film is concentrated in smaller areas and substantial areas of the titanium backing are no longer covered with material. The SEM images (Fig. 8c) confirm these findings. The irradiation has caused the material to shrink.

The RBS (Fig. 9) allowed the elemental composition of the films as a function of layer depth to be determined. The non-irradiated films (Fig. 9a) are dominated by carbon and oxygen, thulium is rather a minor component of the deposits in atomic percentage. The RBS measurements are not sensitive enough to show low amounts of nitrogen or fluorine, however the ERDA measurements on the same samples did show some atomic percentage of nitrogen, from the solvent DMF, and low amounts of fluorine. No sulfur, present in the triflate, was detected, however, both RBS and ERDA, with these parameters are very sensitive to sulfur. The titanium signal scattered from measuring point to measuring point, indicating a heterogeneous distribution

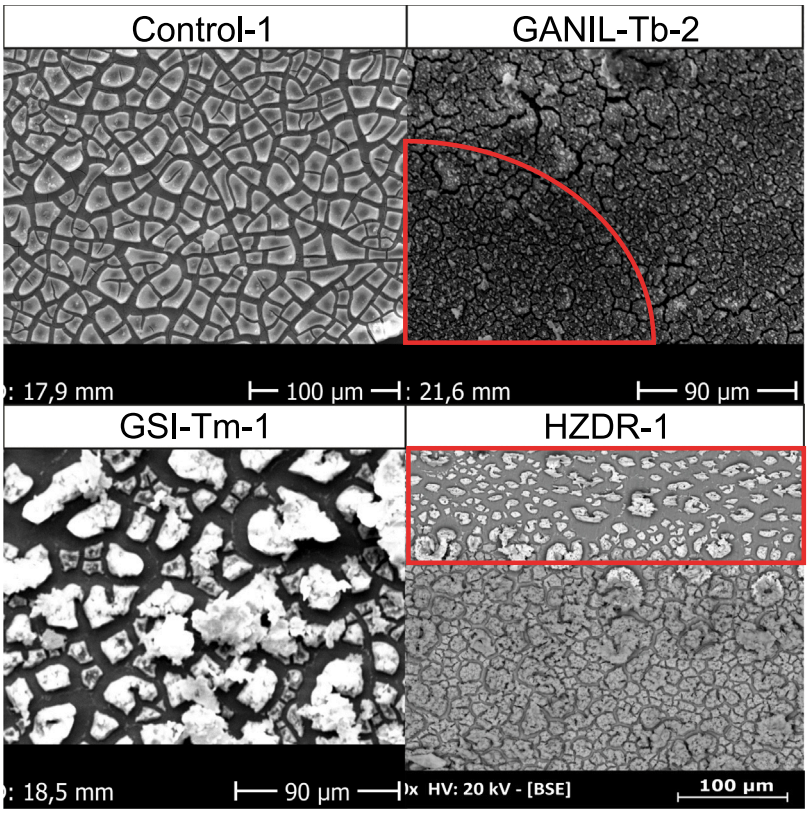

Fig. 5. SEM pictures of different targets are shown. Top left shows Control-1. Top right shows GANIL-Tb-2, which was irradiated at GANIL with 1×10^{14} ^{70}Zn $\frac{\text{ions}}{\text{cm}^2}$ and an energy dose of $2.5(3) \times 10^{8}$ Gy. The red outline shows the area that was hit by the ion beam. Bottom left shows GSI-Tm-1 with a fluence of 2.68×10^{14} ^{48}Ca $\frac{\text{ions}}{\text{cm}^2}$ and an energy dose of $4.5(5) \times 10^{8}$ Gy and bottom right shows HZDR-1 which was irradiated at HZDR with 2×10^{14} ^{35}Cl $\frac{\text{ions}}{\text{cm}^2}$ and an energy of $2.9(3) \times 10^{8}$ Gy . The red outline shows the area that was hit by the ion beam.

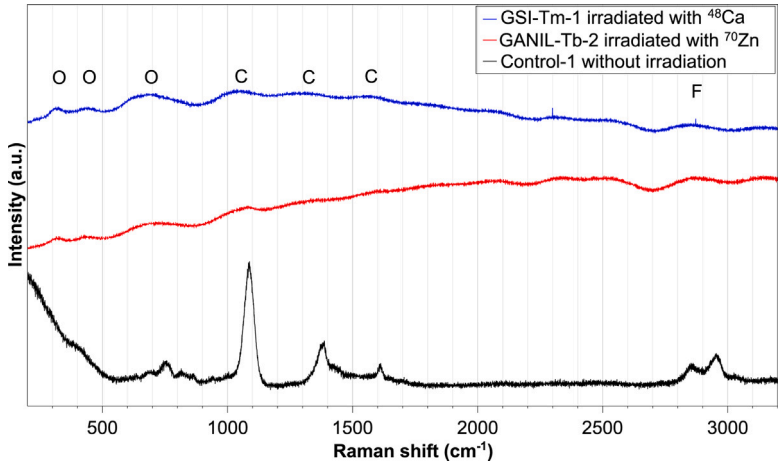

Fig. 6. The Raman spectra of the targets GSI-Tm-1. GANIL-Tb-2 and Control-1. The black spectrum shows an non-irradiated target. The red spectrum shows the vibrational bands after the irradiation with 1×10^{14} $\frac{\text{ions}}{\text{cm}^2}$ ^{70}Zn ions and the blue spectrum shows the vibrational bands after the irradiation with 2.7×10^{14} $\frac{\text{ions}}{\text{cm}^2}$ ^{48}Ca ions. All spectra are normalized to their respective maximum value. Oxides (O), carbonates (C), and formates (F) could be identified in the spectra.

of the thulium film thickness, as also indicated by the PIXE image. With the exception of the titanium signal, the curves were otherwise reproducible for different measuring points.

Through irradiation (Fig. 9b), the carbon signal in the thin films decreases noticeably, while the relative oxygen and thulium content increases. In the layers near the surface of the deposition, the oxygen content is slightly increased compared to the non-irradiated sample area. It should be noted again that glassy carbon was chosen as the anode material in the preparation of these thin films.

The high carbon content could be due to the corrosion of the electrode material.

4. Discussion

4.1. Stability of thin films in ion beams

The thin films exhibited remarkable stability under diverse ion beams and doses, with negligible changes observed during irradiation with a fluence of 1×10^{14} $\frac{\text{ions}}{\text{cm}^2}$ ^{70}Zn and with a fluence of $2.68 \times$

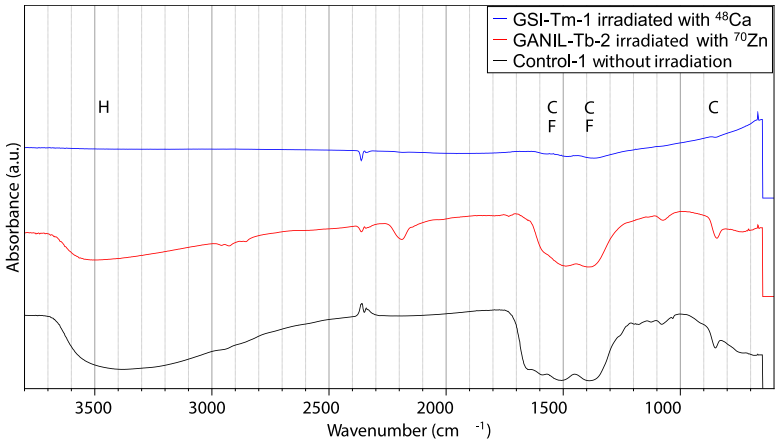

Fig. 7. The IR spectra of the targets GSI-Tm-1. GANIL-Tb-2 and Control-1. The black spectrum shows an non-irradiated target. The red spectrum shows the vibrational bands after the irradiation with 1×10^{14} $\frac{\text{ions}}{\text{cm}^2}$ ^{70}Zn ions and the blue spectrum shows the vibrational bands after the irradiation with 2.7×10^{14} $\frac{\text{ions}}{\text{cm}^2}$ ^{48}Ca ions. All spectra are normalized to their respective maximum value. Hydroxides (H), carbonates (C), and formates (F) could be identified in the spectra.

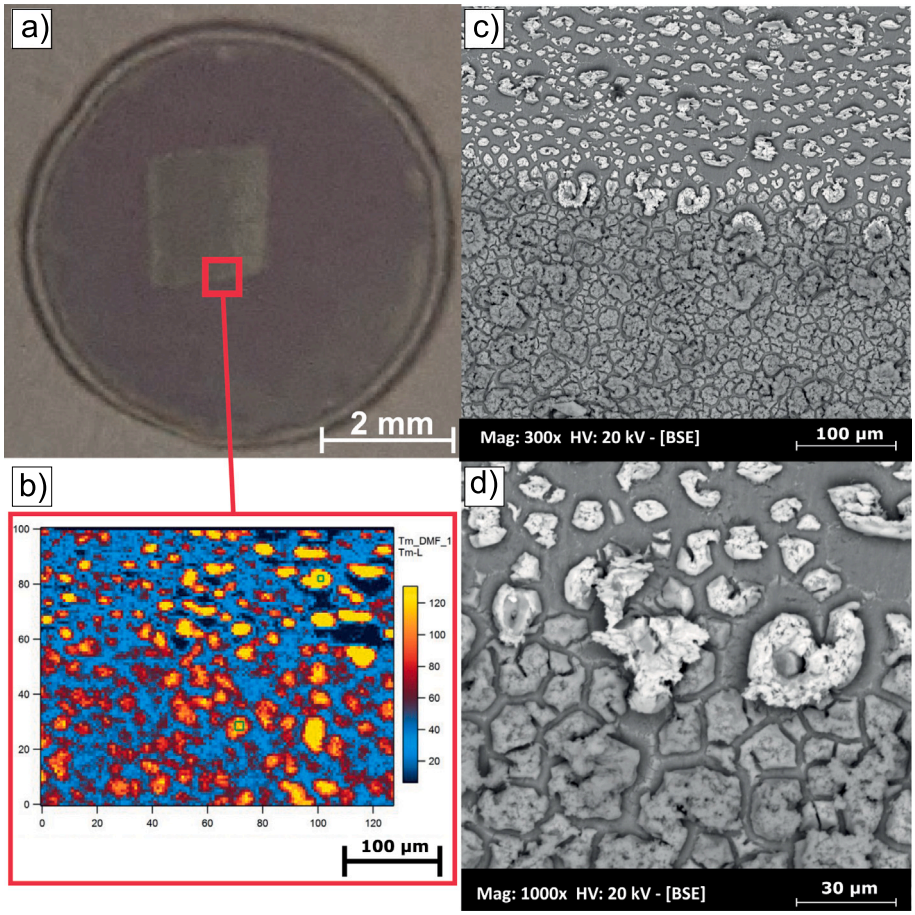

Fig. 8. Images of deposits from HZDR-1 with an estimated surface weight of 1800(200) $\frac{\mu\text{g}}{\text{cm}^2}$ after irradiation at the HZDR. The estimation was done by pre-experiments with a radioactive tracer. (a) Photo of the sample after irradiation with I = 2.0×10^{14} $\frac{\text{ions}}{\text{cm}^2}$ using a 4.9 $\frac{\text{MeV}}{\text{u}}$ $^{35}Cl^{7+}$ ion beam, (b) PIXE image of the boundary between irradiated and non-irradiated thin film, (c) and (d) SEM images of the same region with 300x and 1000x magnification.

10^{14} $\frac{\text{ions}}{\text{cm}^2}$ ^{48}Ca. SEM images revealed only minor morphological changes, suggesting robust stability of the thin films.

The dose applied to all targets are in the same order of magnitude, varying only in a factor of 2–3. This makes every target well comparable to each other.

The ^{48}Ca beam at GSI and the ^{70}Zn beam at GANIL traversed the titanium backing of target sets before hitting the target layer. In contrast, the ^{35}Cl beam was directed at targets HZDR-1, 2, and 3 without passing through the titanium backing. This difference may influence the irradiation damage done to the target thin films. It is noteworthy that variations in post-irradiation behavior of electrodeposited targets, including tile shrinkage [26] or thin film melting [27], have been observed, underscoring the incomplete understanding of these phenomena.

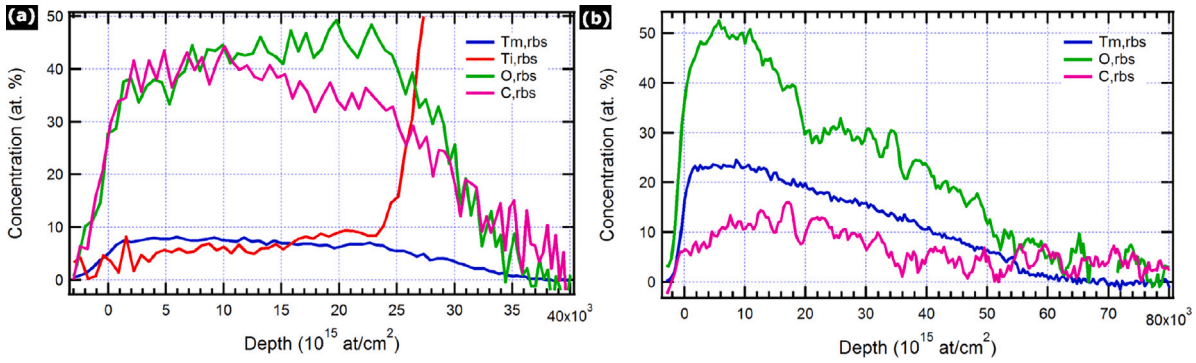

Fig. 9. RBS depth profile of the thin films produced from HZDR-1 under argon atmosphere with an estimated surface weight of 1800(200) $\frac{\mu g}{cm^2}$. The estimation was done by pre-experiments with a radioactive tracer as explained in chapter 2.1.5. (a) before irradiation; (b) after irradiation with I = 2.0×10^{14} $\frac{ions}{cm^2}$ ^{35}Cl.

Comparative analysis, particularly with irradiated MP targets [26, 27], suggests that targets produced via the triflate method hold promise to be at least as stable as those produced via the MP method, even though the fluences are 3 order of magnitude lower compared to typical SHE experiments which have a fluence in the order of magnitude of 1×10^{17} $\frac{ions}{cm^2}$ [28]

4.2. Spectroscopic changes of the thin films

The ERDA measurements did not produce useful results as the method-inherent irradiation with the ^{35}Cl beam led to changes in the layer morphology rather than in further information of the unaltered layer. The applied ion dose corresponded approximately to that of the TASCA experiment, so that the differences in irradiation could then be analyzed in an experiment using the μBeam setup.

PIXE and SEM (Fig. 8) clearly show that the individual tiles of the mudcracking of the thin films are strongly compressed by irradiation. After irradiation they cover significantly less titanium surface of the backing. PIXE and RBS spectra show that the relative amount of thulium in these compacted tiles had increased. RBS spectra (Fig. 9) show that mainly carbon and only little oxygen had been lost through irradiation. The irradiation had thus driven the carbon out of the films. However, it cannot be ruled out that the high carbon content of the non-irradiated thin films comes from corrosion of the anode (glassy carbon). Intercalated solvent (DMF) cannot be ruled out as a cause, since small amounts of nitrogen was observed in the ERDA data but not in the RBS data. Fluorine was visible in small amount in the ERDA measurements but sulfur was completely missing, so that co-deposition of the triflate can be excluded.

The IR and Raman measurements show that targets produced with this method also have organic residues, such as carbonates. Other chemical compounds like carboxylate [6] or formate [8] cannot be clearly detected, but cannot be ruled out either.

As with the MP targets, it can be observed that the carbon-containing species decrease with intensive ion irradiation and oxidic species remain.

Prior to irradiation, the precise chemical composition of the thin film remains unknown. However, as with MP targets, it is hypothesized that organic species, including carbonates, carboxylates and formates, are present in addition to oxide and hydroxide compounds. The irradiation process has been observed to reduce the carbon content, which suggests that the organic components are undergoing destruction and are likely to be escaping as CO_2 in the process. The RBS data from HZDR-1 demonstrate a general decline in carbon content, though it does not reach zero. Organic species, including carbonates and formates, also persist. Simultaneously, the relative oxide content in the RBS measurements for HZDR-1 increases following irradiation. The IR and Raman data of GSI-Tm-1 and GANIL-Tb-2 also demonstrate that the carbon species decrease, though they do not entirely disappear. The Raman data additionally indicates that the oxidic bands remain present, suggesting a transformation of the layer into a purely oxidic film. With higher ion beam intensities, the carbon content is further reduced, indicating that the transformation into a pure oxidic film is not spontaneous but rather a process.

5. Conclusion

The results show that thin films with up to 1600 ± 100 $\frac{\mu g}{cm^2}$ could be produced consistently regardless of the shape and area of the deposition surface. The thin films have demonstrated promising initial results regarding their stability and suitability for use in ion beam experiments.

The targets showed gradual surface and chemical changes with different ion beams and doses. It can be observed that the fraction of carbon-containing species, which were present in the thin films after deposition, decreased after irradiation and the oxidic species became dominant. However, this change occurs relatively slowly. Carbon could still be observed in the film after the irradiation, indicating that this change depends on the energy and fluence of the ion beam. After irradiation with ^{70}Zn, there was an optical change in the GANIL-Tb-1 targets, but this was barely noticeable in SEM compared to the non-irradiated thin films. The structure of GANIL-Tb-1 did not change significantly after irradiation with a ^{70}Zn ion beam with a fluence of 1×10^{14} $\frac{ions}{cm^2}$ under the microscope.

From this it can be concluded that the described method is promising for the production of targets for the production of superheavy elements and that there are prospects that these thin films show stability in the ion beam similar to that of thin films produced using the MP technique.

CRediT authorship contribution statement

E. Artes: Writing – review & editing, Writing – original draft, Visualization, Validation, Project administration, Methodology, Investigation, Formal analysis, Data curation, Conceptualization. **D. Ackermann:** Resources, Investigation. **Ch.E. Düllmann:** Writing – review & editing, Supervision. **T. Häger:** Resources, Investigation. **B. Kindler:** Resources. **T. Lefrou:** Project administration, Investigation. **B. Lommel:** Resources. **A.T. Loria Basto:** Resources, Investigation. **C.-C. Meyer:** Project administration, Methodology, Investigation, Data curation, Conceptualization. **C. Mokry:** Writing – review & editing, Resources. **F. Munnik:** Writing – review & editing, Resources, Investigation, Formal analysis, Data curation. **J. Piot:** Resources, Project administration, Investigation, Data curation, Conceptualization. **L.E. Reed:** Writing – review & editing, Resources, Investigation, Formal analysis, Data curation, Conceptualization. **D. Renisch:** Writing – review & editing, Supervision, Project administration, Investigation, Funding acquisition, Data curation, Conceptualization. **H. Rothard:** Writing – review &

editing, Resources. **J. Runke:** Writing – review & editing, Methodology. **H. Savajols:** Software, Resources, Data curation, Conceptualization. **C. Stodel:** Resources, Project administration, Investigation, Formal analysis, Data curation, Conceptualization. **T. Madi:** Resources. **V. Urbanova:** Resources, Methodology, Investigation. **V. Watt-Morel:** Methodology. **A. Yakushev:** Methodology, Investigation.

Declaration of Generative AI and AI-assisted technologies in the writing process

During the preparation of this work the authors used [ChatGPT GPT-4o] in order to improve the readability and language. After using this tool, the authors reviewed and edited the content as needed and take full responsibility for the content of the published article.

Declaration of competing interest

The authors declare that they have no known competing financial interests or personal relationships that could have appeared to influence the work reported in this paper.

Acknowledgments

Our sincere thanks go to the mechanical workshop at the research reactor TRIGA Mainz for their local support and the financial support from the Helmholtz Institute Mainz. We acknowledge funding from the German Federal Ministry for Research and Education (project 05P21UMFN2). The results presented here are based on the experiment U327, which was performed at the beam line X8/TASCA at the GSI Helmholtzzentrum für Schwerionenforschung, Darmstadt (Germany) in the frame of FAIR Phase-0. The research leading to these results has received funding from the European Union's HORIZON EUROPE Program under grant agreement Nº 101057511. We are grateful to the Ion Beam Center at Helmholtz-Zentrum Dresden-Rossendorf for their support in conducting the ion beam analysis of our samples. Some experiments were performed at the Grand Accélérateur National d'Ions Lourds (GANIL) by means of the CIRIL Interdisciplinary Platform, part of CIMAP laboratory, Caen, France. We thank the staff of CIMAP-CIRIL and GANIL for their invaluable support.

Data availability

Data will be made available on request.

References

[1] O.R. Smits, Ch.E. Düllmann, P. Indelicato, W. Nazarewicz, P. Schwerdtfeger, The quest for superheavy elements and the limit of the periodic table, Nat. Rev. Phys. 6 (2) (2023) 86–98, http://dx.doi.org/10.1038/s42254-023-00668-y.

[2] Y.Ts. Oganessian, Heaviest nuclei from ^{48}Ca-induced reactions, J. Phys. G: Nucl. Part. Phys. 34 (4) (2007) R165–R242, http://dx.doi.org/10.1088/0954-3899/34/4/r01.

[3] Ch.E. Düllmann, et al., Advancements in the fabrication and characterization of actinide targets for superheavy element production, J. Radioanal. Nucl. Chem. 332 (5) (2023) 1505–1514, http://dx.doi.org/10.1007/s10967-022-08631-4.

[4] E. Artes, Ch.E. Düllmann, C.-C. Meyer, D. Renisch, The process of molecular plating and the characteristics of the produced thin films – what we have learned in 60 years and what is still unknown, EPJ Web Conf. 285 (2023) 03001, http://dx.doi.org/10.1051/epjconf/202328503001.

[5] W. Parker, R. Falk, Molecular plating: A method for the electrolytic formation of thin inorganic films, Nucl. Instrum. Methods 16 (1962) 355–357, http://dx.doi.org/10.1016/0029-554x(62)90142-8.

[6] A. Vascon, et al., Elucidation of constant current density molecular plating, Nucl. Instrum. Methods Phys. Res. Sect. A 696 (2012) 180–191, http://dx.doi.org/10.1016/j.nima.2012.08.072.

[7] K. Eberhardt, et al., Preparation of targets for the gas-filled recoil separator TASCA by electrochemical deposition and design of the TASCA target wheel assembly, Nucl. Instrum. Methods Phys. Res. Sect. A 590 (1–3) (2008) 134–140, http://dx.doi.org/10.1016/j.nima.2008.02.069.

[8] C.-C. Meyer, et al., Fabrication, swift heavy ion irradiation, and damage analysis of lanthanide targets, Radiochim. Acta 111 (11) (2023) 801–815, http://dx.doi.org/10.1515/ract-2023-0197.

[9] M.E.M. Hamidi, J.-L. Pascal, Synthesis and structural characterization of some anhydrous Ln(OTf)$_3$ complexes (Ln=Sc, La, Nd, Sm, Gd and Er OTf=CF_3SO_3, Polyhedron 13 (11) (1994) 1787–1792, http://dx.doi.org/10.1016/s0277-5387(00)80111-4.

[10] J. Runke, et al., Preparation of actinide targets for the synthesis of the heaviest elements, J. Radioanal. Nucl. Chem. 299 (2) (2013) 1081–1084, http://dx.doi.org/10.1007/s10967-013-2616-6.

[11] E. Jäger, et al., High intensity target wheel at TASCA: target wheel control system and target monitoring, J. Radioanal. Nucl. Chem. 299 (2) (2013) 1073–1079, http://dx.doi.org/10.1007/s10967-013-2645-1.

[12] C. Stodel, et al., High intensity targets stations for S3, J. Radioanal. Nucl. Chem. 305 (3) (2015) 761–767, http://dx.doi.org/10.1007/s10967-015-3936-5.

[13] H. Rothard, CIRIL: Interdisciplinary research at GANIL, Nucl. Phys. News 32 (1) (2022) 29–33, http://dx.doi.org/10.1080/10619127.2021.1990680.

[14] A. Gurbich, SigmaCalc recent development and present status of the evaluated cross-sections for IBA, Nucl. Instrum. Methods Phys. Res. Sect. B 371 (2016) 27–32, http://dx.doi.org/10.1016/j.nimb.2015.09.035.

[15] N.P. Barradas, C. Jeynes, R.P. Webb, Simulated annealing analysis of Rutherford backscattering data, Appl. Phys. Lett. 71 (2) (1997) 291–293, http://dx.doi.org/10.1063/1.119524.

[16] W.B. White, V.G. Keramidas, Vibrational spectra of oxides with the C-type rare earth oxide structure, Spectrochim. Acta Part A 28 (3) (1972) 501–509, http://dx.doi.org/10.1016/0584-8539(72)80237-x.

[17] R.L. Frost, et al., Effect of the lanthanide ionic radius on the Raman spectroscopy of lanthanide agardite minerals, J. Raman Spectrosc. 35 (11) (2004) 961–966, http://dx.doi.org/10.1002/jrs.1243.

[18] R.L. Frost, A. López, R. Scholz, Y. Xi, F.M. Belotti, Infrared and Raman spectroscopic characterization of the carbonate mineral huanghoite – And in comparison with selected rare earth carbonates, J. Mol. Struct. 1051 (2013) 221–225, http://dx.doi.org/10.1016/j.molstruc.2013.07.051.

[19] L. Spiridigliozzi, et al., An in-depth multi-technique characterization of rare earth carbonates $Re_2(CO_3)3{\cdot}2H_2O$ owning tengerite-type structure, J. Rare Earths 40 (8) (2022) 1281–1290, http://dx.doi.org/10.1016/j.jre.2021.09.020.

[20] R.L. Frost, M.J. Dickfos, Raman spectroscopy of halogen-containing carbonates, J. Raman Spectrosc. 38 (11) (2007) 1516–1522, http://dx.doi.org/10.1002/jrs.1806.

[21] E.N. Silva, et al., Vibrational modes of rare-earth formates, J. Raman Spectrosc. 40 (8) (2009) 954–957, http://dx.doi.org/10.1002/jrs.2207.

[22] V. Kartha, S. Venkateswaran, Vibrational spectra and normal vibrations of rare earth formates, Spectrochim. Acta, Part A 37 (11) (1981) 927–934, http://dx.doi.org/10.1016/0584-8539(81)80017-7.

[23] O.D. Saralidze, L.P. Shklover, K.I. Petrov, V.E. Plyushchev, Infrared absorption spectra of formates of the rare earth elements, J. Struct. Chem. 8 (1) (1967) 45–49, http://dx.doi.org/10.1007/bf00741723.

[24] J. de Hosson, The infrared spectra of several rare-earth formates, J. Inorg. Nucl. Chem. 37 (11) (1975) 2350–2351, http://dx.doi.org/10.1016/0022-1902(75)80753-6.

[25] P.V. Klevtsov, R.F. Klevtsova, L.P. Sheina, Relationship between the infrared absorption spectra and crystal structure of the hydroxides of the rare earth elements and yttrium, J. Struct. Chem. 8 (2) (1967) 229–233, http://dx.doi.org/10.1007/bf00745638.

[26] C.-C. Meyer, et al., Microscopic and spectroscopic analysis of ion-irradiated molecular-plated thin films for super-heavy element production, Nucl. Instrum. Methods Phys. Res. Sect. A (2024) accepted.

[27] D. Mayorov, E. Tereshatov, T. Werke, M. Frey, C. Folden, Heavy-ion beam induced effects in enriched gadolinium target films prepared by molecular plating, Nucl. Instrum. Methods Phys. Res. Sect. B 407 (2017) 256–264, http://dx.doi.org/10.1016/j.nimb.2017.07.012.

[28] J. Khuyagbaatar, et al., ^{48}Ca + ^{249}Bk fusion reaction leading to element Z=117: Long-lived α-decaying ^{270}Db and discovery of ^{266}Lr, Phys. Rev. Lett. 112 (17) (2014) 172501, http://dx.doi.org/10.1103/physrevlett.112.172501.